# Efficient generation and tight focusing of radially polarized beam from linearly polarized beam with all-dielectric metasurface

**Fei Zhang, Honglin Yu,[*] Jiawen Fang, Ming Zhang, Sicheng Chen, Jian Wang, Anguo He, and Junyan Chen**

*Key Laboratory of Optoelectronic Technology and System, Ministry of Education, Chongqing University, Chongqing 400030, China*
*[*]hlyu@cqu.edu.cn*

**Abstract:** We propose a single layer all-dielectric metasurface lens to simultaneously convert and focus an incident linear polarization into a radial beam with high efficiency and high numerical aperture (NA). It shows a better focusing property compared with the linearly polarized metasurface lens for high NA. A tight spot size (0.502λ) is achieved for the NA = 0.94. Additionally, the emergent polarization can in principle be switched flexibly between radially and azimuthally polarized beams by the adjustment of incident polarization direction. It is expected that our scheme may have potential value in microscopy, material processing, medicine, particles accelerating and trapping, and so on.

## References and links

1. K. Youngworth and T. Brown, "Focusing of high numerical aperture cylindrical-vector beams," Opt. Express **7**(2), 77–87 (2000).
2. W. Chen and Q. Zhan, "Three-dimensional focus shaping with cylindrical vector beams," Opt. Commun. **265**(2), 411–417 (2006).
3. Q. Zhan, "Cylindrical vector beams: from mathematical concepts to applications," Adv. Opt. Photonics **1**(1), 1–57 (2009).
4. H. P. Urbach and S. F. Pereira, "Field in focus with a maximum longitudinal electric component," Phys. Rev. Lett. **100**(12), 123904 (2008).
5. R. Dorn, S. Quabis, and G. Leuchs, "Sharper focus for a radially polarized light beam," Phys. Rev. Lett. **91**(23), 233901 (2003).
6. L. Yang, X. Xie, S. Wang, and J. Zhou, "Minimized spot of annular radially polarized focusing beam," Opt. Lett. **38**(8), 1331–1333 (2013).
7. A. Cheng, J. T. Gonçalves, P. Golshani, K. Arisaka, and C. Portera-Cailliau, "Simultaneous two-photon calcium imaging at different depths with spatiotemporal multiplexing," Nat. Methods **8**(2), 139–142 (2011).
8. Q. Zhan, "Evanescent Bessel beam generation via surface plasmon resonance excitation by a radially polarized beam," Opt. Lett. **31**(11), 1726–1728 (2006).
9. C. Varin and M. Piché, "Acceleration of ultra-relativistic electrons using high-intensity TM01 laser beams," Appl. Phys. B **74**(S1), S83–S88 (2002).
10. M. Meier, V. Romano, and T. Feurer, "Material processing with pulsed radially and azimuthally polarized laser radiation," Appl. Phys., A Mater. Sci. Process. **86**(3), 329–334 (2007).
11. O. J. Allegre, W. Perrie, S. P. Edwardson, G. Dearden, and K. G. Watkins, "Laser microprocessing of steel with radially and azimuthally polarized femtosecond vortex pulses," J. Opt. **14**(8), 085601 (2012).
12. G. Machavariani, Y. Lumer, I. Moshe, A. Meir, and S. Jackel, "Efficient extracavity generation of radially and azimuthally polarized beams," Opt. Lett. **32**(11), 1468–1470 (2007).
13. W. J. Lai, B. C. Lim, P. B. Phua, K. S. Tiaw, H. H. Teo, and M. H. Hong, "Generation of radially polarized beam with a segmented spiral varying retarder," Opt. Express **16**(20), 15694–15699 (2008).
14. C. R. Doerr and L. L. Buhl, "Circular grating coupler for creating focused azimuthally and radially polarized beams," Opt. Lett. **36**(7), 1209–1211 (2011).
15. C. F. Phelan, J. F. Donegan, and J. G. Lunney, "Generation of a radially polarized light beam using internal conical diffraction," Opt. Express **19**(22), 21793–21802 (2011).
16. H. Chen, J. Hao, B.-F. Zhang, J. Xu, J. Ding, and H.-T. Wang, "Generation of vector beam with space-variant distribution of both polarization and phase," Opt. Lett. **36**(16), 3179–3181 (2011).

17. J. Qi, X. Li, W. Wang, X. Wang, W. Sun, and J. Liao, "Generation and double-slit interference of higher-order vector beams," Appl. Opt. **52**(34), 8369–8375 (2013).
18. Q. Zhan and J. Leger, "Focus shaping using cylindrical vector beams," Opt. Express **10**(7), 324–331 (2002).
19. H. Wang, L. Shi, B. Lukyanchuk, C. Sheppard, and C. T. Chong, "Creation of a needle of longitudinally polarized light in vacuum using binary optics," Nat. Photonics **2**(8), 501–505 (2008).
20. G. H. Yuan, S. B. Wei, and X.-C. Yuan, "Nondiffracting transversally polarized beam," Opt. Lett. **36**(17), 3479–3481 (2011).
21. X.-C. Yuan, J. Lin, J. Bu, and R. E. Burge, "Achromatic design for the generation of optical vortices based on radial spiral phase plates," Opt. Express **16**(18), 13599–13605 (2008).
22. M. Pu, Z. Zhao, Y. Wang, X. Li, X. Ma, C. Hu, C. Wang, C. Huang, and X. Luo, "Spatially and spectrally engineered spin-orbit interaction for achromatic virtual shaping," Sci. Rep. **5**, 9822 (2015).
23. X. Ni, S. Ishii, A. V. Kildishev, and V. M. Shalaev, "Ultra-thin, planar, Babinet-inverted plasmonic metalenses," Light Sci. Appl. **2**(4), e72 (2013).
24. D. Tang, C. Wang, Z. Zhao, Y. Wang, M. Pu, X. Li, P. Gao, and X. Luo, "Ultrabroadband superoscillatory lens composed by plasmonic metasurfaces for subdiffraction light focusing," Laser Photonics Rev. **9**(6), 713–719 (2015).
25. J. Lin, J. P. Mueller, Q. Wang, G. Yuan, N. Antoniou, X.-C. Yuan, and F. Capasso, "Polarization-controlled tunable directional coupling of surface plasmon polaritons," Science **340**(6130), 331–334 (2013).
26. X. Luo, M. Pu, X. Ma, and X. Li, "Taming the electromagnetic boundaries via metasurfaces: from theory and fabrication to functional devices," Int. J. Antennas Propag. **2015**, 204127 (2015).
27. M. Kang, J. Chen, X.-L. Wang, and H.-T. Wang, "Twisted vector field from an inhomogeneous and anisotropic metamaterial," J. Opt. Soc. Am. B **29**(4), 572–576 (2012).
28. J. Lin, P. Genevet, M. A. Kats, N. Antoniou, and F. Capasso, "Nanostructured holograms for broadband manipulation of vector beams," Nano Lett. **13**(9), 4269–4274 (2013).
29. J. Luo, Z. Zhao, M. Pu, N. Yao, D. Tang, P. Gao, J. Jin, X. Li, C. Wang, H. Yu, and X. Luo, "Tight focusing of radially and azimuthally polarized light with plasmonic metalens," Opt. Commun. **356**, 445–450 (2015).
30. F. Monticone, N. M. Estakhri, and A. Alù, "Full control of nanoscale optical transmission with a composite metascreen," Phys. Rev. Lett. **110**(20), 203903 (2013).
31. F. Aieta, P. Genevet, M. A. Kats, N. Yu, R. Blanchard, Z. Gaburro, and F. Capasso, "Aberration-free ultrathin flat lenses and axicons at telecom wavelengths based on plasmonic metasurfaces," Nano Lett. **12**(9), 4932–4936 (2012).
32. C. Pfeiffer and A. Grbic, "Cascaded metasurfaces for complete phase and polarization control," Appl. Phys. Lett. **102**(23), 231116 (2013).
33. Z. Wei, Y. Cao, X. Su, Z. Gong, Y. Long, and H. Li, "Highly efficient beam steering with a transparent metasurface," Opt. Express **21**(9), 10739–10745 (2013).
34. J. Luo, H. Yu, M. Song, and Z. Zhang, "Highly efficient wavefront manipulation in terahertz based on plasmonic gradient metasurfaces," Opt. Lett. **39**(8), 2229–2231 (2014).
35. A. Arbabi, Y. Horie, A. J. Ball, M. Bagheri, and A. Faraon, "Subwavelength-thick lenses with high numerical apertures and large efficiency based on high-contrast transmitarrays," Nat. Commun. **6**, 7069 (2015).
36. A. Arbabi, Y. Horie, M. Bagheri, and A. Faraon, "Dielectric metasurfaces for complete control of phase and polarization with subwavelength spatial resolution and high transmission," Nat. Nanotechnol. **10**(11), 937–943 (2015).
37. J. van de Groep and A. Polman, "Designing dielectric resonators on substrates: combining magnetic and electric resonances," Opt. Express **21**(22), 26285–26302 (2013).
38. F. Gori, "Measuring Stokes parameters by means of a polarization grating," Opt. Lett. **24**(9), 584–586 (1999).
39. W. Moriaki, K. Keiei, and S. Takehisa, *Physical Properties and Data of Optical Materials* (Beijing: Chemical Industry Press, 2010), in Chinese.
40. Q. Zhan, "Trapping metallic Rayleigh particles with radial polarization: reply to comment," Opt. Express **20**(6), 6058–6059 (2012).
41. B. Richards and E. Wolf, "Electromagnetic diffraction in optical systems. II. Structure of the image field in an aplanatic system," Proc. R. Soc. Lond. A Math. Phys. Sci. **253**(1274), 349 (1959).
42. R. Dorn, S. Quabis, and G. Leuchs, "The focus of light—linear polarization breaks the rotational symmetry of the focal spot," J. Mod. Opt. **50**, 1917–1926 (2003).

## 1. Introduction

During the past decades, the cylindrical vector beams have received particular attention for their notable high-numerical-aperture focusing properties [1–3]. Especially, the strong longitudinal electric field component is of existence at the focus of radially polarized (RP) beam [4], leading to a sharper focal spot than a homogeneously polarized beam [5,6], which results in many significant applications in high-resolution microscopy [7], surface plasmon excitation [8], particles accelerating [9], material processing [10,11], and so on. Typically, some traditional methods, such as radial or azimuthal polarization converter [5,6], segmented waveplates [12], segmented spiral varying retarder [13], circular grating coupler [14], internal conical diffraction [15], and spatial light modulators [16,17], have been utilized to generate

radially or azimuthally polarized (AP) light. However, the methods mentioned above are somewhat bulky, unstable, or low efficiency. Furthermore, the applications of the focused AP beam based on conventional spherical lens and annular apertures are limited by their size, planarity and volume [18–20]. As a result, it is of difficulty to meet the need for miniaturization and integration.

Many recent studies have focused on the artificial structures with subwavelength scale and abrupt phase change, in virtue of their unprecedented ability to flexibly modify the wavefront of electromagnetic wave in combination with miniaturization and integration. Thus, lots of optical devices have been generated, for instance, spiral phase plates [21,22], flat meta-lenses [23,24], plasmonic metasurface elements [25,26], *etc*. To begin with, the RP or AP beam has been generated by some specific metasurfaces with circularly polarized light illumination [27,28]. Then, the plasmonic meta-lens with arrayed metal nanoantennas has been reported and posses the capability of focusing RP or AP beam into a spot [29]. However, it encounters the difficulty of keeping the centers of the cylindrical vector beam and meta-lens coaxial, and this type of single-layer plasmonic metasurfaces suffer from the low transmission or polarization conversion efficiency because of fundamental limits [27–30] and metal absorption loss [31,32]. Furthermore, some multi-layer structures seem to offer a high efficiency [32–34], but they need further improvement for massive practical applications due to the problems like alignment of multi-layer patterns in processing. Finally, most of dielectric metasurfaces with high efficiency could only focus the incident light without polarization conversion [35]. There is no all-dielectric meta-lens that can simultaneously generate and focus RP beam into a tight spot from linearly polarized beam with high efficiency and high NA, although it has been reported that a metasurface could provide complete control of polarization and phase [36]. As a result, abovementioned shortcomings pose obstacles for practical applications of RP beam.

Here, a single-layer meta-lens, which is based on high-contrast dielectric elliptical posts, is designed to simultaneously generate and focus RP (or AP) beam into a focal spot (or doughnut-shaped focus) from *x*- (or *y*-) polarized beam with high efficiency and high NA. The emergent polarization can be switched conveniently between RP and AP beams by adjusting incident polarization direction. The polarization conversion is achieved ingeniously by introducing one phase difference of $\pi$ between two special orthogonal polarizations of linearly polarized incident light. Thus, it could solve the problem of the harshly coaxial condition in practical applications. Moreover, it shows a better focusing property compared with the linearly polarized metasurface lens consisting of dielectric cylinder posts for high NA. A tight spot size (0.502λ) is obtained when the designed meta-lens with NA of 0.94 is illuminated with *x*-polarized light at 10.6 μm. We believe that our scheme may have potential applications in microscopy, material processing, medicine, particles accelerating and trapping, *etc*.

## 2. Structure model design

A typical periodic hexagonal unit cell and its geometry parameters are shown in Fig. 1(a). It is composed of a layer barium fluoride substrate ($BaF_2$) and a silicon (Si) elliptical post with an orientation $\theta$. To analyze its mechanism, we employed the finite integral technique (FIT) based on CST Microwave Studio to obtain the magnetic energy density in periodic posts, as shown in Fig. 1(b). The optical energy concentrated within the posts proves that each post can be regarded as a waveguide truncated on both sides and work as a weakly coupled low-quality-factor Fabry-Pérot resonator [36], mainly owing to the high refractive index contrast between the Si posts and their surroundings [35–37]. Thus, it results in different effective refractive indices and phase shifts ($\phi_x$ and $\phi_y$), which almost do not vary with orientation of the post [36], of two waveguide modes polarized along the ellipse diameters. As a result, each unit cell can operate as a local wave-plate with an optical axis $\theta$. By proper selections of two ellipse diameters, we can realize discretional combination of $\phi_x$ and $\phi_y$ ranging from *0* to *2π* while maintaining high transmissions. We believe that such a capability is of importance for the generation of RP beam.
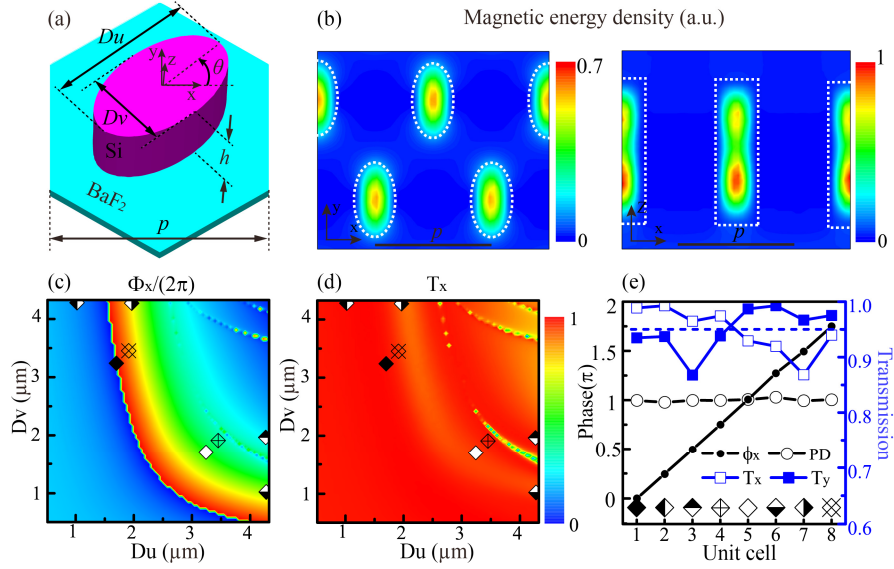
Fig. 1. (a) Schematic three-dimensional view of a unit cell. The refraction indexes of substrate and post are 1.396 and 3.418 [39], respectively. $\theta$ is an orientation of the silicon elliptical post. Other parameters: $p = 5.15$ μm, $h = 6.6$ μm. (b) The color-coded magnetic energy density when $x$-polarized light is normally incident from the substrate of periodic posts. The dashed white lines denote the boundary of the silicon posts. (left: $x$-$y$ cross-section at 3.3 μm above the BaF$_2$-Si interface; right: $x$-$z$ cross-section; parameters: $Du = 1.91$ μm, $Dv = 3.45$ μm, $\theta = 0$). (c) and (d) The phase shift ($\phi_x$) and transmission ($T_x$) as a function of the elliptical post diameters ($Du$ and $Dv$) for $x$-polarized light. The color-coded image of $\phi_y$ (or $T_y$) for $y$-polarized incident light is a mirrored image of that of $\phi_x$ in (c) (or $T_x$ in (d)) flipped along the $Du = Dv$. (e) The phase shift ($\phi_x$), transmissions ($T_x$ and $T_y$) and phase difference ($PD$) between $x$ and $y$ polarization excitation of the eight unit cells. The elliptical post diameters ($Du$ and $Dv$) of unit cells from 1 to 4 are $Du = 1.7$, 1.02, 4.27 and 3.45 μm, and $Dv = 3.24$, 4.28, 1.96 and 1.91 μm. The blue shot dash line presents an average transmission of 0.95. The unit cells from 5 to 8 are acquired by rotating the elliptical posts from 1 to 4 by an angle of 90° clockwise.

Each unit cell can behave as a local half-wave plate when there is a phase difference of $\pi$ between the two linear polarizations aligned to the ellipse axes. Considering one linearly polarized beam normally propagating through an array of half-wave plates, whose fast axes form an angle $\varphi/2$ (where $\varphi = \arctan(y/x)$ is the azimuthal angle) by the $x$ axis, the Jones matrix **G** showing the transformation of the structure, as follows [38]:

$$\mathbf{G} = \eta \begin{bmatrix} \cos\varphi & \sin\varphi \\ \sin\varphi & -\cos\varphi \end{bmatrix}. \tag{1}$$

where we consider the transmission amplitudes of the two-diameter direction as equal because of little difference, and $\eta$ is the transmission amplitude of transmission light. The normal incident $x$- and $y$-polarized light, after passing the abovementioned structure, can be transformed into the following electric field, respectively:

$$\mathbf{E} = \eta E_0 \exp(jkz)[\cos\varphi, \sin\varphi, 0]. \tag{2}$$

$$\mathbf{E} = \eta E_0 \exp(jkz)[\sin\varphi, -\cos\varphi, 0]. \tag{3}$$

where $E_0$ is the amplitude of incident electric field; $k = 2\pi/2$ is the wave vector. It is obvious that Eqs. (2) and (3) are the electric field vector of RP and AP light denoted in Cartesian coordinate, respectively. An arbitrary linear polarization light can be decomposed

into two orthogonal *x*- and *y*-polarized lights, so the emergent polarization can in principle be switched between RP and AP beams by changing the polarization direction of the linearly polarized incident beam.

To get the relationship between the elliptical post diameters (*Du* and *Dv*) and the phase shifts ($\phi_x$ and $\phi_y$), *x*- and *y*-polarized light at 10.6 μm are utilized to illuminate a periodic array of elliptical posts ($\theta = 0$), respectively. Moreover, the phase shifts ($\phi_x$ and $\phi_y$) and transmissions ($T_x$ and $T_y$) are performed based on FIT as a function of the elliptical post diameters, as shown in Fig. 1(c) and 1(d) respectively. We choose eight different elliptical posts with a phase difference of ~π between the two linearly polarized transmission light aligned to the ellipse axes as well as an incremental phase of π/4 between adjacent posts with an average transmission higher than 95%, as illustrated inset of Fig. 1(c) and 1(d). The phase shift ($\phi_x$), phase difference (*PD*) and transmissions ($T_x$ and $T_y$) of the eight unit cells are shown in Fig. 1(e). The transmissions are approximately equal. Thus, each unit cell can be considered as a local half-wave plate.
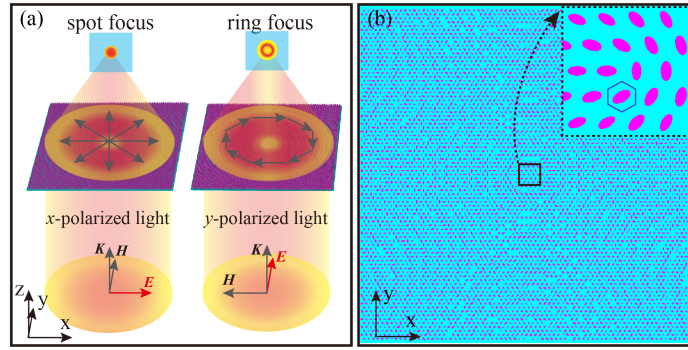


Fig. 2. (a) Schematic representation of generating and focusing RP (or AP) light from *x*- (or *y*-) polarized light. A focal spot can come into being for *x*-polarized incident beam; a ring focus can be obtained for *y*-polarized incident beam. (b) The schematic of the designed planar A-lens with size of 385 μm × 385 μm and focal length of 70 μm. Insets: expanded view of the A-lens.

In order to obtain a gradient meta-lens for generating and focusing RP (or AP) light into a focal spot (or doughnut-shaped focus) from *x*- (or *y*-) polarized light as shown in Fig. 2(a), the eight unit cells in Fig. 1(e) are arrayed by undergoing a parabolic phase distribution $\phi(x,y)$ in Eq. (4), and then rotating around their local positions with an angle $\varphi/2$ to modify local polarization directions. The relationship between the phase distribution of unit cells $\phi(x, y)$ and the location center coordinate *x* and *y* is given by:

$$\phi(x, y) = -2n\pi + k(\sqrt{x^2 + y^2 + f^2} - f). \tag{4}$$

where *f* is the focal length of the meta-lens; *n* is an arbitrary integer number. According to Youngworth's formulas [1] in combination with Eqs. (2) and (3), the normal incident *x*- and *y*-polarized light, after passing the meta-lens, can be converted into the following electric field, respectively:

$$\mathbf{E} = \eta E_0 \exp(jk\sqrt{x^2 + y^2 + f^2}) \begin{bmatrix} \cos\alpha\cos\varphi \\ \cos\alpha\sin\varphi \\ \sin\alpha \end{bmatrix}. \tag{5}$$

$$\mathbf{E} = \eta E_0 \exp(jk\sqrt{x^2 + y^2 + f^2}) \begin{bmatrix} \sin\varphi \\ -\cos\varphi \\ 0 \end{bmatrix}. \tag{6}$$

where $\alpha = \arcsin \sqrt{(x^2 + y^2)/(x^2 + y^2 + f^2)}$ is the deflection angle for local position.

## 3. Simulation results and analysis

In order to validate the analytical model and extend the theoretical analysis, according to the design approach mentioned above, a 2D flat RP and AP meta-lens (we call it A-lens later in this paper) has been designed as shown in Fig. 2(b), whose size and focal length are 385 μm × 385 μm and 70 μm (NA = 0.94) respectively. We simulate the whole 3D lens using FIT based on CST at the wavelength of 10.6 μm and then compare with the results in theory. To this end, the transient solver is used along with an extremely fine hexahedral mesh with a minimum mesh size of 0.1μm (0.009λ) and a total number of ~239 × 10⁶ mesh cells. Furthermore, about 46.6 × 10⁶ mesh cells are used to capture field behavior in the elliptical posts. In the system and simulation, the numerical aperture is defined as $NA = \sin[\arctan(D/2f)]$, where $D$ is the width of the lens.
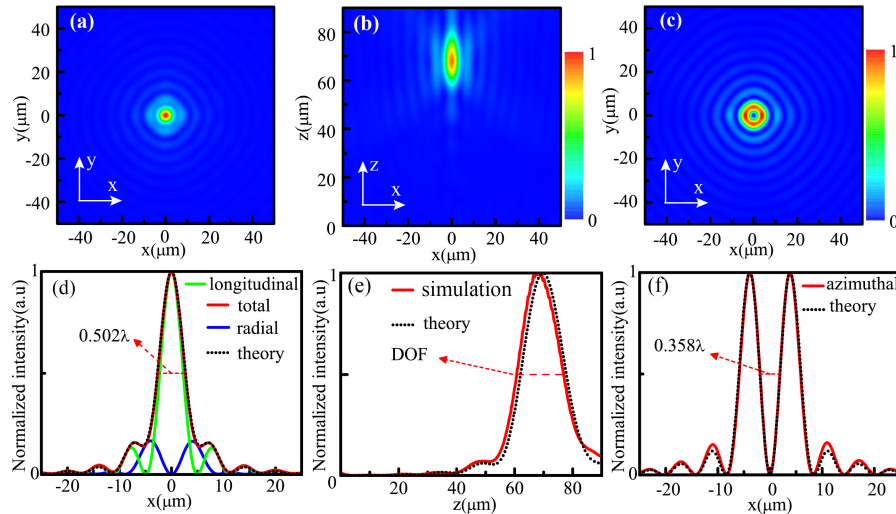


Fig. 3. (a) and (b) Two views of focused cross-sections ($z$ = 69.3 μm and $y$ = 0 plane) for $x$-polarized incident light. (c) The cross-sectional intensity profile at the focal plane ($z$ = 69.3 μm) for $y$-polarized incident light. (d)-(f) The sectional intensity profiles of simulation and theory calculations: (d) for $x$-polarized incident beam at the focus along the $x$-axis; (e) for $x$-polarized incident beam along the optical axis; (f) for $y$-polarized incident beam at the focus along the $x$-axis. The theory and simulation results in (d) and (f) are compared at different distances from the lens but at the focal points of each one ($z$ = 69.3 μm for simulation, $z$ = 69.8 μm for theory).

A circular spot focus is obtained in the focal plane when the designed A-lens is illuminated with $x$-polarized light as illustrated in Fig. 3(a), thanks to the polarization symmetry of RP beam. The cross-sectional intensity profile of electric field at the focal plane is the sum of radial component and longitudinal component (owing to polarization conversion and deflection by the array of posts). The green, blue and red solid curves in Fig. 3(d) signify the simulated intensity profiles of longitudinal component, radial component and total field, respectively. The full width at half maximum (FWHM) and center position of focal spot are ~5.321 μm (0.502λ) and ~69.3 μm (with a focal shift ~1%; the theoretical focal length is ~69.8 μm), which approach to the diffractive limit and designed focal length, respectively. Figure 3(b) shows the cross-sectional intensity profile in the $xz$ plane; Fig. 3(e) illustrates the intensity profiles of simulation and theory calculations along the optical axis. The depth of focus (DOF, which is defined as the FWHM along the optical axis) is ~16.2 μm (the theoretical value is ~15.8 μm). The maximum focused electric field is ~32.6 times that of the incident field. Furthermore, the efficiency of focus is ~39%, which is defined as the ratio of

the power in the main focal spot region to the total input power before the lens. The black dot curves in Fig. 3(d) and 3(e) are the normalized intensity distributions of theory calculation, which is also based on the Youngworth's formulas [1] in Eq. (7), at the focal plane along the $x$-axis and along the optical axis, respectively.

$$\mathbf{E} = \int_{-y_{max}}^{y_{max}} \int_{-x_{max}}^{x_{max}} \eta E_0 \exp(jk\sqrt{x^2 + y^2 + f^2}) \begin{bmatrix} \cos\alpha\cos\varphi \\ \cos\alpha\sin\varphi \\ \sin\alpha \end{bmatrix} dxdy. \tag{7}$$

where $x_{max}$ and $y_{max}$ are the maximum values of transverse coordinate for the designed meta-lens, respectively.

For $y$-polarized beam, a hollow dark spot is attainable in the focal plane as shown in Fig. 3(c). There is only the azimuthal component (stemming from polarization conversion by the array of posts) at the focus. Obviously, the dark center of doughnut focus suggests that the longitudinal component is not available for $y$-polarized incident light; the electric field is purely transverse and zero at the center. Thus, there is the strong magnetic field on the optical axis, which could be utilized in optical trapping and manipulation of particles [40]. The red solid line and black dot curve in Fig. 3(f) denote the normalized intensity distributions of simulation and theory calculations at the focal points of each one along the $x$-axis, respectively. The peak-to-peak distance (PP) is ~7.727 μm (0.729λ), and the corresponding FWHM of doughnut focus is ~3.792 μm (0.358λ). The focusing efficiency is ~49%. The formula of theory calculation is given by:

$$\mathbf{E} = \int_{-y_{max}}^{y_{max}} \int_{-x_{max}}^{x_{max}} \eta E_0 \exp(jk\sqrt{x^2 + y^2 + f^2}) \begin{bmatrix} \sin\varphi \\ -\cos\varphi \\ 0 \end{bmatrix} dxdy. \tag{8}$$

According to the analyses above in combination with Fig. 3(d)-3(f), there is good consistency between the simulation and theory results, which provides strong evidence for the correctness of the theoretical analysis and simulated results.

In order to make a comparison with the RP meta-lens, we designed another linearly polarized meta-lens (we call it B-lens later in this article) consisted of cylinders posts, whose arrangement, materials and geometry parameters (except the relationship between the phase shift and the diameter) are the same as A-lens shown in Fig. 1(b). It focuses linearly polarized beam without polarization conversion, owing to the circular symmetry of silicon cylinder. Figure 4(a) shows the transmission and phase shift for this periodic structure as a function of the duty cycle (the ratio of the post diameter to the lattice constant) at the wavelength of 10.6 μm.

On the basis of FIT simulations, three focused cross-sections of the designed B-lens with NA = 0.94 and $f$ = 70 μm at the $z$ = 69.3 μm, $y$ = 0 and $x$ = 0 plane are presented in Figs. 4(b)-4(d) for $x$-polarized incident light at 10.6 μm. The FWHM along the $x$ and $y$ direction are ~7.477 μm (0.705λ) and ~4.544 μm (0.429λ), respectively. The maximum focused electric field is ~37.6 times that of the incident field, and the focusing efficiency is ~34%. An asymmetry focus comes into being in the focal plane as showing in Fig. 4(b) with a focal shift ~1%, which was predicted by Richards and Wolf in 1959 [41] and experimentally verified in traditional optical systems [42]. Because the longitudinal $z$ component is cancelled by interference in the focal region and varies with the azimuthal angle φ, which makes its intensity distribution depressed at the focus and show maxima away from the optical axis in the $x$ direction as illustrated in Fig. 4(c) and 4(d), leading to the asymmetry of the total field.
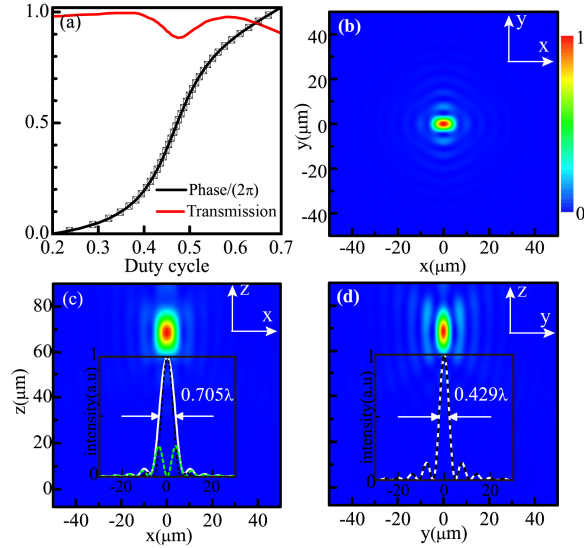
Fig. 4. (a) Simulated transmission and phase shift of a 2D periodic array of silicon cylinders in a hexagonal lattice. (b-d) Three views of focused cross-sections ($z$ = 69.3 μm, $y$ = 0 and $x$ = 0 plane) for B-lens. The cross-sectional intensity distributions at the $z$ = 69.3 μm plane along the $x$ and $y$ direction are illustrated in (c) and (d), respectively. The black and green shot dash lines, and the white solid curve in the insets depict the normalized intensity of the $x$ component, longitudinal $z$ component, and total field, respectively.

Figure 5 shows that the focal shifts ($FS_1$ and $FS_2$), maximum focused amplitudes ($A_1$ and $A_2$), focusing efficiencies ($E_1$ and $E_2$) and FWHM ($Fx_1$, $Fx_2$ and $Fy_2$) of two different types of meta-lenses (A-lens and B-lens) vary with different NA values for the same focal length of 70 μm (only by changing the width of the lens) when the meta-lenses are illuminated with $x$-polarized light at 10.6 μm. As the NA increases, the focusing efficiencies, FWHM and focal shifts of two types of meta-lenses show a decreasing trend, but their focused intensities get reinforced. Under small NA condition, both FWHM and focal shift of B-lens are obviously smaller than A-lens. Also, its focusing efficiency and focused intensity are larger than A-lens. Because the tangential electric field energy, which plays a leading role in the total energy for
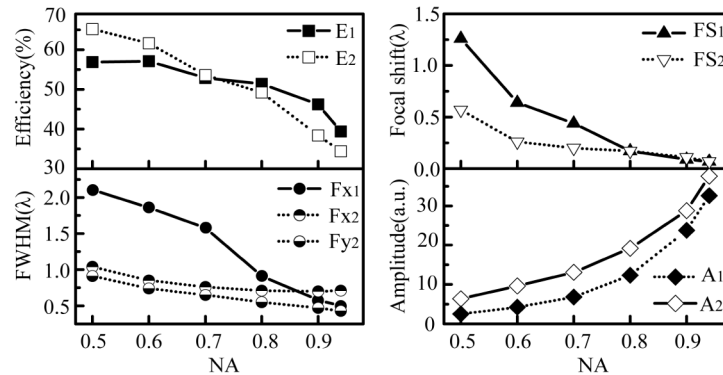


Fig. 5. The focusing efficiency ($E_1$ and $E_2$), FWHM ($Fx_1$, $Fx_2$ and $Fy_2$), focal shift ($FS_1$ and $FS_2$) and maximum focused amplitude ($A_1$ and $A_2$) of two different types of meta-lenses (A-lens and B-lens) vary with different NA values. Here, $FS_1$, $A_1$, $E_1$ and $Fx_1$ present the focusing features of A-lens.

small NA, is cancelled by interference in the focal region for A-lens. However, under high NA condition, the efficiencies, focal shifts and focused intensities of two types of meta-lenses

have no obvious difference, but the <mark>focal spot of A-lens is sharper</mark> and more symmetrical than that of B-lens, mainly thanks to the polarization conversion from linear to radial and the existence of a greater proportion of longitudinal $z$ component in the focal region of the focused RP beam. In brief, the results of analysis verify that A-lens shows a better focusing property for high NA.

## 4. Conclusion

In conclusion, we utilize the method of abrupt phase shift to achieve simultaneous control of polarization and phase with an a<mark>verage transmission higher than 95%.</mark> A novel meta-lens has been designed for $x$- (or $y$-) polarized incident light to simultaneously generate and focus RP (or AP) beam into a symmetry spot focus (or doughnut focus) with high efficiency and high NA. It shows a <mark>better focusing property</mark> compared with the linearly polarized metasurface lens for high NA. A tight spot size ($0.502\lambda$) is obtained when the designed meta-lens with NA of 0.94 is illuminated with $x$-polarized light at 10.6 μm. Additionally, the emergent polarization can in principle be switched between RP and AP beams by changing the incident polarization direction. It is expected that our scheme have many potential applications such as microscopy, material processing, medicine, particles accelerating and trapping, *etc*.

## Acknowledgments